nature neuroscience

Regulatory T cells promote myelin regeneration in the central nervous system

Yvonne Dombrowski[1], Thomas O'Hagan[1], Marie Dittmer[1], Rosana Penalva[1], Sonia R Mayoral[2], Peter Bankhead[3], Samara Fleville[1], George Eleftheriadis[1], Chao Zhao[4], Michelle Naughton[1], Rachel Hassan[1], Jill Moffat[1], John Falconer[1], Amanda Boyd[5], Peter Hamilton[3], Ingrid V Allen[1], Adrien Kissenpfennig[1], Paul N Moynagh[1,6], Emma Evergren[3], Bernard Perbal[7,8], Anna C Williams[5], Rebecca J Ingram[1], Jonah R Chan[2], Robin J M Franklin[4] & Denise C Fitzgerald[1]

Regeneration of CNS myelin involves differentiation of oligodendrocytes from oligodendrocyte progenitor cells. In multiple sclerosis, remyelination can fail despite abundant oligodendrocyte progenitor cells, suggesting impairment of oligodendrocyte differentiation. T cells infiltrate the CNS in multiple sclerosis, yet little is known about T cell functions in remyelination. We report that regulatory T cells (T_{reg}) promote oligodendrocyte differentiation and (re)myelination. T_{reg}-deficient mice exhibited substantially impaired remyelination and oligodendrocyte differentiation, which was rescued by adoptive transfer of T_{reg}. In brain slice cultures, T_{reg} accelerated developmental myelination and remyelination, even in the absence of overt inflammation. T_{reg} directly promoted oligodendrocyte progenitor cell differentiation and myelination *in vitro*. We identified CCN3 as a T_{reg}-derived mediator of oligodendrocyte differentiation and myelination *in vitro*. These findings reveal a new regenerative function of T_{reg} in the CNS, distinct from immunomodulation. Although the cells were originally named 'T_{reg}' to reflect immunoregulatory roles, this also captures emerging, regenerative T_{reg} functions.

The failure to reinvest demyelinated axons with new myelin sheaths results in a lack of axonal conduction and metabolic support. This ultimately leads to irreversible axonal loss, which typifies later stages of chronic demyelinating diseases such as multiple sclerosis (MS), leaving patients with permanent neurological disability[1,2]. Remyelination frequently occurs in the context of innate and adaptive immune responses[3,4]. T cells can act as effectors of myelin damage but are also required for successful remyelination[5]. However, T cells encompass a range of phenotypically and functionally distinct subsets, and the contributions of T cell subsets to CNS remyelination are poorly understood. Since inflammation-resolving effects of T_{reg} frequently coincide with tissue regeneration, we hypothesized that T_{reg} promote remyelination.

RESULTS

T_{reg} cells are required for efficient oligodendrocyte progenitor cell differentiation during remyelination *in vivo*.

To study regenerative T cell functions in remyelination *in vivo*, as distinct from classical T cell-mediated demyelination observed in experimental autoimmune encephalomyelitis (EAE), focal demyelination was induced by injecting lysolecithin into spinal cord white matter of mice. Such lesions naturally remyelinate within 1 month and follow a well-defined time-course with distinct phases of oligodendrocyte progenitor cell (OPC) activation, recruitment and oligodendrocyte differentiation[6,7]. Flow cytometric immunophenotyping 3 d post lesioning (d.p.l.) demonstrated an abundance of $CD45^+CD11b^+$ myeloid cells in lesioned tissue, as previously described[8]. However, distinct (albeit smaller) populations of $CD3^+$ and $CD4^+$ T cells were also evident even up to 11 d.p.l., including $CD3^+CD4^+Foxp3^+$ T_{reg}, a T cell population recently implicated in tissue regeneration[9,10] (**Supplementary Fig. 1a–e**). To determine whether T_{reg} were functionally important in remyelination, we used Foxp3-DTR transgenic mice in which diphtheria toxin (DT) administration depletes Foxp3-expressing cells[11] (**Supplementary Fig. 1f**). Chronic DT exposure causes toxicity and considerable morbidity even in wild-type mice[12–14], while T_{reg} deficiency induces systemic immune activation[11], precluding long-term studies. Therefore, densities of $CC1^+Olig2^+$-differentiated oligodendrocytes, a surrogate readout of remyelination[15], were compared at 14 d.p.l., and electron microscopy was performed at 17 d.p.l.

T_{reg}-depleted animals exhibited significantly fewer differentiated $CC1^+Olig2^+$ oligodendrocytes than nondepleted animals or DT-treated wild-type controls (**Fig. 1a**,**b**). Mice lacking T_{reg} exhibited comparable lesion sizes (**Fig. 1c**), indicating that T_{reg} were not required

[1]Centre for Experimental Medicine, School of Medicine, Dentistry and Biomedical Science, Queen's University Belfast, Northern Ireland, UK. [2]Department of Neurology and Program in Neurosciences, University of California, San Francisco, California, USA. [3]Centre for Cancer Research and Cell Biology, School of Medicine, Dentistry and Biomedical Science, Queen's University Belfast, Northern Ireland, UK. [4]Wellcome Trust-Medical Research Council Cambridge Stem Cell Institute, Clifford Allbutt Building, Cambridge Biomedical Campus, University of Cambridge, UK. [5]Centre for Regenerative Medicine, University of Edinburgh, Edinburgh, UK. [6]Institute of Immunology, Department of Biology, National University of Ireland Maynooth, Ireland. [7]Université Côte d'Azur, CNRS, GREDEG, Nice, France. [8]International CCN Society, Paris, France. Correspondence should be addressed to D.C.F. (d.fitzgerald@qub.ac.uk).

Received 22 August 2016; accepted 3 February 2017; published online 13 March 2017; doi:10.1038/nn.4528

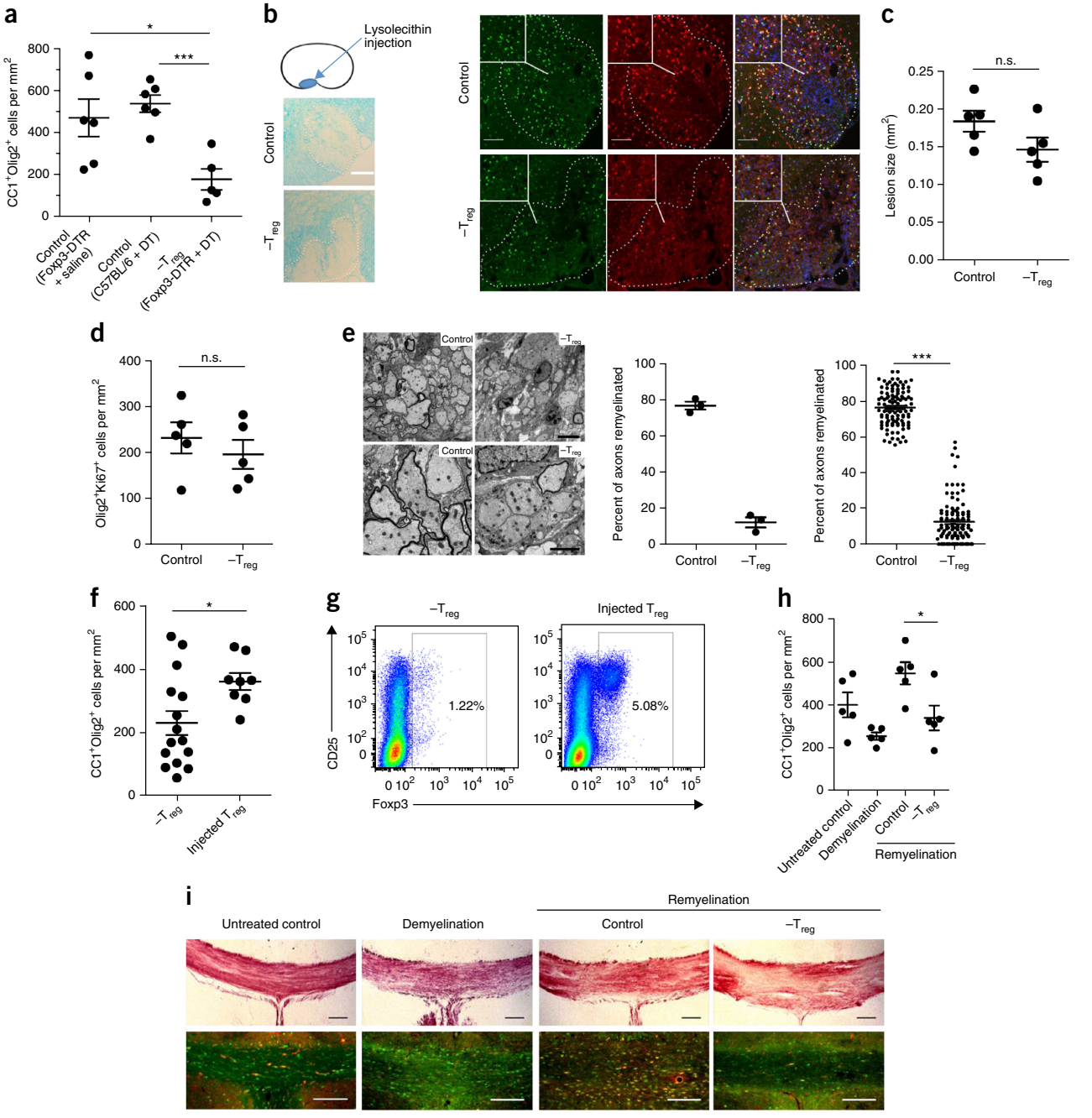

Figure 1 T_{reg} are required for efficient OPC differentiation and remyelination *in vivo*. (**a**) Immunohistochemical analysis of $CC1^+Olig2^+$ cells per lesion area in spinal cords of Foxp3-DTR and C57BL/6 mice at 14 d.p.l.; $n = 6$ control mice and $n = 5$ T_{reg}-depleted ($-T_{reg}$) mice ($t = 2.703$, d.f. = 9, $^*P = 0.0243$; $t = 5.624$, d.f. = 9, $^{***}P = 0.0003$). (**b**) Representative images of **a** showing demyelination by Luxol fast blue staining (scale bar, 200 µm) and $CC1^+Olig2^+$ cells in lesions (scale bar, 100 µm; green, $Olig2^+$ cells; red, $CC1^+$ cells; blue, DAPI). Rightmost panels: merged images. (**c**) Lesion size of Foxp3-DTR mice ± DT at 5 d.p.l. ($n = 5$ mice per group; $t = 1.773$, d.f. = 8, $P = 0.1142$). (**d**) $Olig2^+Ki67^+$ cells per lesion area in spinal cords of Foxp3-DTR mice at 5 d.p.l. ($n = 5$ mice per group; $t = 0.7789$, d.f. = 8, $P = 0.4584$). (**e**) Left: electron micrographs showing distribution of remyelinated axons vs. unmyelinated axons in spinal cord lesions of control or T_{reg}-depleted mice at 17 d.p.l. Scale bar, 5 µm (top) and 1 µm (bottom). Middle: three mice per group were analyzed. Right: data represent mean ± s.e.m. from 109 micrographs from 3 mice per group (two-tailed Mann-Whitney *U*-test; $U = 2$, $P < 0.0001$). (**f**) $CC1^+Olig2^+$ cells per lesion area in spinal cords of DT-treated Foxp3-DTR mice with or without adoptively transferred T_{reg} at 14 d.p.l. ($n = 15$ T_{reg}-depleted mice and $n = 8$ T_{reg}-depleted and adoptively transferred T_{reg} mice pooled from two independent experiments; $t = 2.353$, d.f. = 21, $P = 0.0285$). (**g**) Representative flow cytometric identification of adoptively transferred T_{reg} in lymph nodes of T_{reg}-injected mice from **f** and controls, gated on $CD4^+$ cells (gray box, $Foxp3^+$ cells; colors indicate density of events, ranging from low (blue) to high (red) density). (**h**) Immunohistochemical analysis of $CC1^+Olig2^+$ cells per area of the corpus callosum 2 weeks after cuprizone withdrawal ($n = 5$ mice per group; data represent analysis of 1–2 regions of corpus callosum per mouse; $t = 2.693$, d.f. = 8, $P = 0.0274$). (**i**) Representative images of **h**. Top: Black Gold II myelin stain. Bottom: $Olig2^+CC1^+$ cell staining (green, $Olig2^+$ cells; red, $CC1^+$ cells; scale bar, 100 µm). Data shown are representative of 4 (**a** and **b**), 2 (**c**, **d**, **f** and **g**) and 1 (**e**, **h** and **i**) independent biological experiments. Data presented with mean values as indicated; error bars show s.e.m.; unpaired two-tailed Student's *t*-test, unless otherwise indicated above. $^*P < 0.05$, $^{***}P < 0.001$; n.s., not significant.

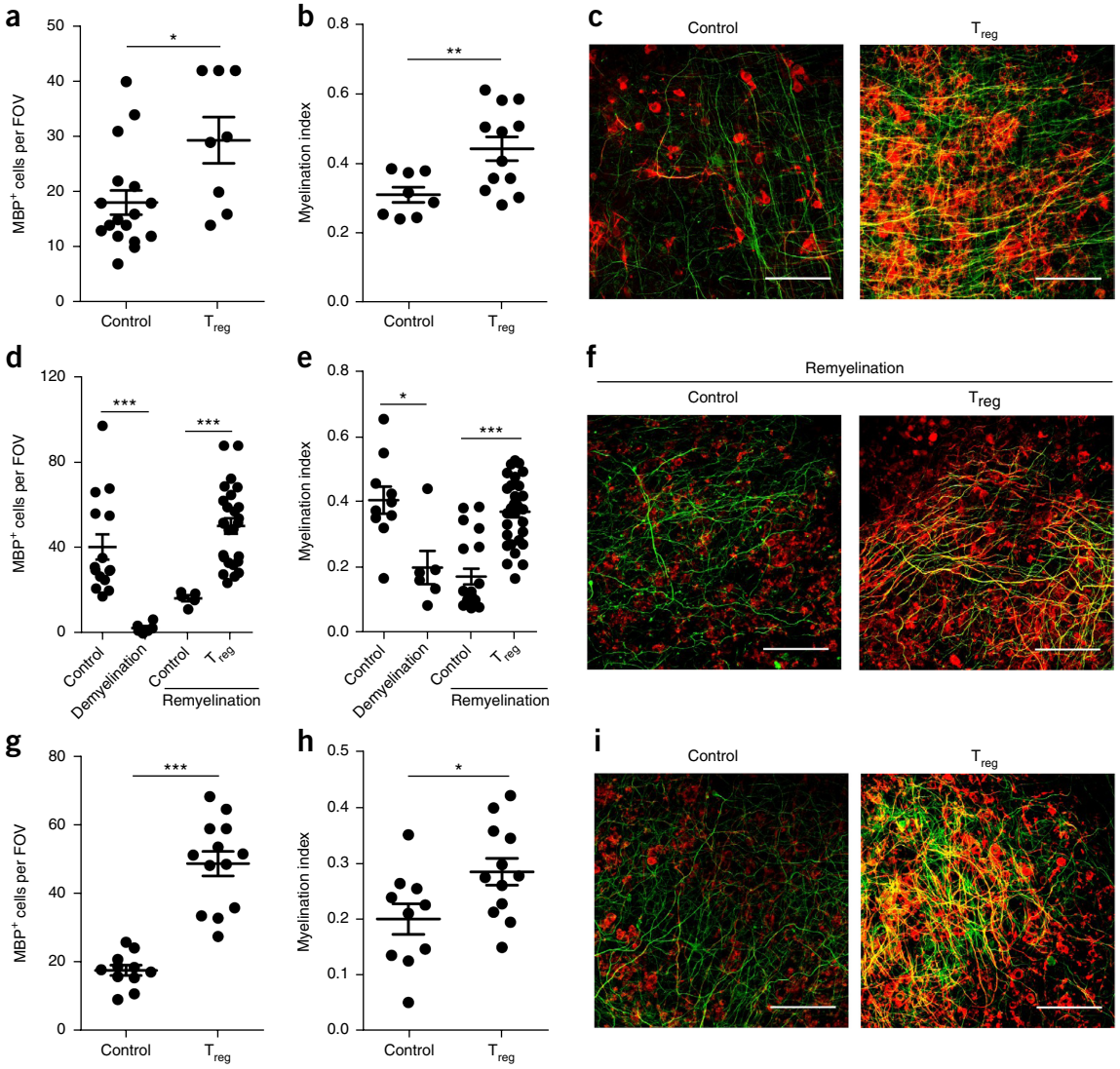

Figure 2 T_{reg} directly promote brain tissue myelination and remyelination *ex vivo*. (**a**–**c**) Analysis of (**a**) MBP$^+$ cells and (**b**) myelination index per field of view (FOV) in brain stem slices treated with control media or T_{reg}-conditioned media. (**c**) Representative images taken from *z*-stacks at 7 d.i.v. (scale bar, 100 µm; green, neurofilament-200 (NF200); red, MBP). Control: MBP$^+$ counts, $n = 17$ FOV and myelination index, $n = 8$ FOV. T_{reg}: MBP$^+$ counts, $n = 8$ and myelination index, $n = 12$ FOV. FOVs were selected from 3 or 4 slices per group (MBP$^+$ counts: $U = 28.5$, $P = 0.0196$, two-tailed Mann-Whitney *U*-test; myelination index: $t = 2.886$, d.f. = 18, $P = 0.0098$, unpaired two-tailed Student's *t*-test). (**d**–**f**) Analysis of (**d**) MBP$^+$ cells and (**e**) myelination index per FOV in control, demyelinated and remyelinating brain stem slices. (**f**) Representative images taken from *z*-stacks (scale bar, 100 µm; green, NF200; red, MBP). Control: MBP$^+$ counts, $n = 15$ FOV and myelination index, $n = 10$ FOV. Demyelination: MBP$^+$ counts, $n = 6$ FOV and myelination index, $n = 6$ FOV. Remyelination control: MBP$^+$ counts, $n = 5$ FOV and myelination index, $n = 20$ FOV. Remyelination + T_{reg}: MBP$^+$ counts, $n = 26$ and myelination index, $n = 32$ FOV. Fields of view were selected from 3–6 slices per group (MBP$^+$ counts: demyelination, $U = 0$, $P < 0.0001$; remyelination, $U = 0$, $P < 0.0001$; two-tailed Mann Whitney *U*-test; myelination index: demyelination, $U = 9$, $P = 0.0225$; two-tailed Mann Whitney *U*-test, remyelination, $t = 5.845$, d.f. = 50, $P = 0.001$; unpaired two-tailed Student's *t*-test). (**g**–**i**) Analysis of (**g**) MBP$^+$ cells and (**h**) myelination index per FOV in brain stem slices. (**i**) Representative images taken from *z*-stacks (scale bar, 100 µm; green, NF200; red, MBP). Control: MBP$^+$ counts, $n = 11$ FOV and myelination index, $n = 10$ FOV. T_{reg}: MBP$^+$ counts, $n = 13$ and myelination index, $n = 12$ FOV. FOVs were selected from 3–6 slices per group (MBP$^+$ counts: $t = 7.537$, d.f. = 22, $P < 0.0001$; myelination index: $t = 2.334$, d.f. = 20, $P = 0.0301$, unpaired two-tailed Student's *t*-tests). Data shown are representative of 6 (**a**–**c**) and 2 (**d**–**f** and **g**–**i**) independent experiments. Data presented with mean values as indicated; error bars indicate s.e.m.; $^*P < 0.05$, $^{**}P < 0.01$, $^{***}P < 0.001$.

to limit tissue damage in this model and, notably, that experimental groups had comparable burdens of demyelination to repair. Reduced numbers of CC1$^+$Olig2$^+$ cells in T_{reg}-depleted mice could have arisen because of a failure to recruit sufficient OPC to the demyelinated area. However, no significant differences in Olig2$^+$Ki67$^+$-proliferating OPC at 5 d.p.l. or 10 d.p.l. were observed between groups (**Fig. 1d** and **Supplementary Fig. 1g**), indicating that reduced generation of oligodendrocytes was likely due to impairment in differentiation. Restricting T_{reg} depletion only to the prelesioning phase did not alter CC1$^+$Olig2$^+$ cell numbers (**Supplementary Fig. 1h**), suggesting that T_{reg} were important in later stages of remyelination. Indeed, electron microscopic analysis of lesions demonstrated significantly fewer remyelinated axons in T_{reg}-depleted animals (**Fig. 1e**). To further test the role of T_{reg} in remyelination using a gain-of-function model, magnetic-activated cell sorting (MACS)-purified wild-type T_{reg} were injected into T_{reg}-deficient animals ('injected T_{reg}'). T_{reg} administration

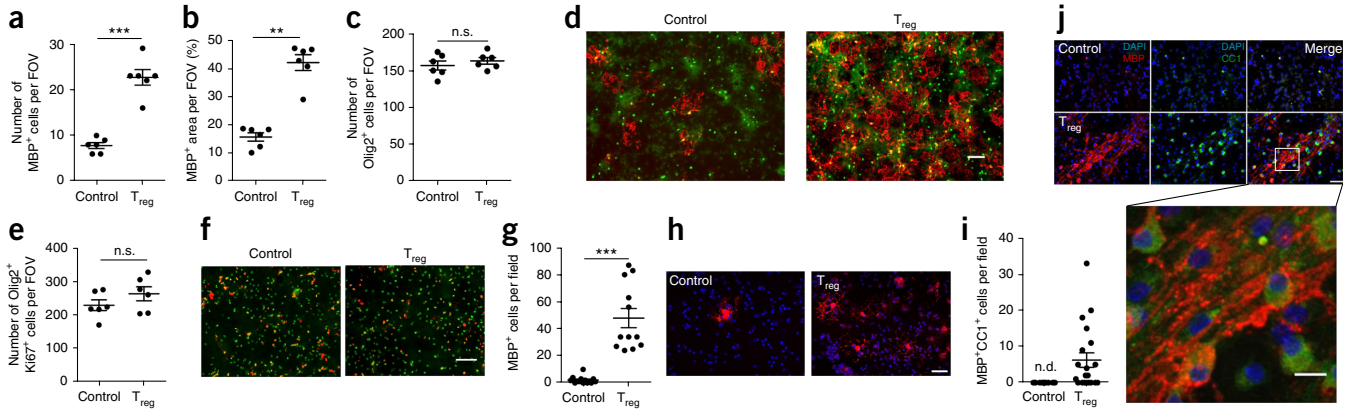

Figure 3 T_{reg} directly enhance oligodendrocyte differentiation and myelination *in vitro*. (**a**–**d**) Immunofluorescence analysis of (**a**) MBP+ cell numbers ($t = 8.200$, d.f. = 10, $P < 0.0001$), (**b**) percentage area ($U = 0$, $P = 0.0022$), (**c**) total Olig2+ cell numbers ($t = 0.8294$, d.f. = 10, $P = 0.4263$) and (**d**) representative images of mixed glial cultures analyzed (scale bar, 100 µm; green, Olig2; red, MBP; $n = 6$ wells). (**e**,**f**) Immunofluorescence analysis of (**e**) Olig2+Ki67+ cell numbers ($t = 1.299$, d.f. = 10, $P = 0.2230$) with (**f**) representative images of mixed glial cultures (scale bar, 100 µm; green, Olig2; red, Ki67, $n = 6$ wells). (**g**,**h**) Immunofluorescence analysis of (**g**) MBP+ cell numbers ($t = 6.431$, d.f. = 22, $P < 0.0001$) and (**h**) representative images of pure OPC cultures analyzed (scale bar, 50 µm; red, MBP; blue, DAPI, $n = 12$ FOVs). (**i**,**j**) Immunofluorescence analysis of (**i**) MBP+CC1+cell numbers (n.d., not detectable) and (**j**) representative images of DRG neuron–OPC cocultures in the presence or absence of T_{reg}-conditioned medium ($n = 20$ fields of view; scale bars, 50 µm and 20 µm (enlarged image); red, MBP; green, CC1; blue, DAPI). Data shown are representative of at least 12 (**a**, **b** and **d**), 3 (**c** and **g**–**j**) and 2 (**e** and **f**) independent experiments. Data presented with mean values as indicated; error bars show s.e.m.; unpaired two-tailed Student's *t*-test (cell counts) and Mann-Whitney *U*-tests (percentage area); ** $P < 0.01$, *** $P < 0.001$; n.s., not significant.

significantly increased numbers of CC1+Olig2+-differentiated oligodendrocytes in lesions, demonstrating the capacity of T_{reg} to rescue impaired oligodendrocyte differentiation *in vivo* (**Fig. 1f**,**g**). To verify the importance of T_{reg} in myelin regeneration in a second remyelinating model, as well as at a different CNS site, demyelination was induced using cuprizone. Similarly to results obtained using the spinal cord lysolecithin model, T_{reg} depletion significantly impaired CC1+Olig2+ oligodendrocyte differentiation in the corpus callosum of cuprizone-treated mice at day 14 of the remyelination phase (**Fig. 1h**,**i**) but not at day 10 (**Supplementary 1i**). This finding was supported by reduced *Plp1* mRNA expression in T_{reg}-depleted animals at day 14 (**Supplementary Fig. 1j**). T_{reg}-depletion did not significantly affect overall oligodendrocyte lineage numbers (**Supplementary Fig. 1k**; $P = 0.2857$ at day 10 and $P = 0.1273$ at day 14), emphasizing the predominant effect of T_{reg}-depletion on the differentiation phase of the regenerative response. To our knowledge, these studies identify a novel functional role for T_{reg} in the process of oligodendrocyte differentiation and CNS remyelination in both brain and spinal cord *in vivo*.

T_{reg} directly promote brain tissue myelination and remyelination *ex vivo*.

Next, we asked if T_{reg} exerted direct regenerative effects within CNS tissue, distinct from immunomodulation of infiltrating immune cells. To this end, we used neonatal murine organotypic brain slice cultures that naturally generate compact myelin *ex vivo* via OPC proliferation, differentiation and axonal ensheathment[16–19]. To determine whether T_{reg} influenced myelination, fluorescence-activated cell sorting (FACS)-purified CD4+Foxp3-eGFP+ natural T_{reg} or control CD4+Foxp3− conventional T cells were added directly onto slices. T cells infiltrated tissues and GFP+ T_{reg} were still detectable within slices after 3 d *in vitro* (d.i.v.) (**Supplementary Fig. 2a**). Slices co-cultured with T_{reg} cells contained significantly more MBP+ oligodendrocytes and had significantly higher myelination index (myelin and axonal overlap, representing axonal ensheathment by myelin) at 3 d.i.v. than control slices without added cells (**Supplementary Fig. 2b–d**; $P = 0.0041$ and $P = 0.0033$) or slices with conventional T cells (**Supplementary Fig. 2e**; $P = 0.0006$). These findings demonstrate a myelinating action induced specifically by T_{reg}, rather than by activated T cells in general.

To investigate mechanisms of T_{reg}-induced myelination beyond cell–cell contact, slices were supplemented either with control medium or with conditioned media from CD4+ T cells that were polarized to a T_{reg} phenotype or that were nonpolarized to serve as activated T cell controls (**Supplementary Fig. 2f**). T_{reg}-conditioned media significantly increased MBP+ mature oligodendrocytes and myelination compared to controls at 7 d.i.v. (**Fig. 2a–c** and **Supplementary Fig. 2g**). These findings indicated that secreted factors drive oligodendrocyte differentiation and promyelinating effects of T_{reg}.

To test if T_{reg} also promoted regeneration of myelin, slices were myelinated in culture for 14 d and were then demyelinated with lysolecithin for 16 h. Addition of T_{reg}-conditioned media for 7 d following demyelination significantly increased MBP+ mature oligodendrocytes (**Fig. 2d**,**f**) and myelination index (**Fig. 2e**,**f** and **Supplementary Videos 1** and **2**) compared to controls. These increases represented an acceleration of remyelination by T_{reg}, as control slices eventually remyelinated after 2 weeks (data not shown). This was confirmed by electron microscopy showing significantly increased numbers of remyelinated axons in T_{reg}-treated slices compared to control remyelinating slices (**Supplementary Fig. 2h–j**; $P = 0.0016$ and $P = 0.0381$).

Although brain slices lack peripheral immune cells, CNS-resident microglia and astrocytes can generate local inflammatory responses upon slicing and demyelination[20,21], and therefore, effects of T_{reg} on (re)myelination could be due to known anti-inflammatory functions. Thus, to categorically test whether T_{reg} directly promoted CNS myelination rather than indirectly via immunoregulation, slices were equilibrated for 1 week after slicing to allow proinflammatory cytokine production to subside[20] (**Supplementary Fig. 2k**) before addition of T cell-conditioned media for 7 d. In this model, slices treated with T_{reg}-conditioned media again exhibited significantly higher MBP+ oligodendrocyte numbers (**Fig. 2g**,**i**) and myelination index (**Fig. 2h**,**i**) than controls. These findings show that T_{reg} directly promoted

oligodendrocyte differentiation and myelin production under minimally inflammatory conditions, suggesting a primary regenerative function of T_{reg} in the CNS distinct from, but complementary to, known immunomodulatory functions.

T_{reg} directly enhance oligodendrocyte differentiation and myelination *in vitro*.

To further investigate mechanisms of T_{reg}-induced remyelination via OPC differentiation, we next determined whether T_{reg} directly influenced

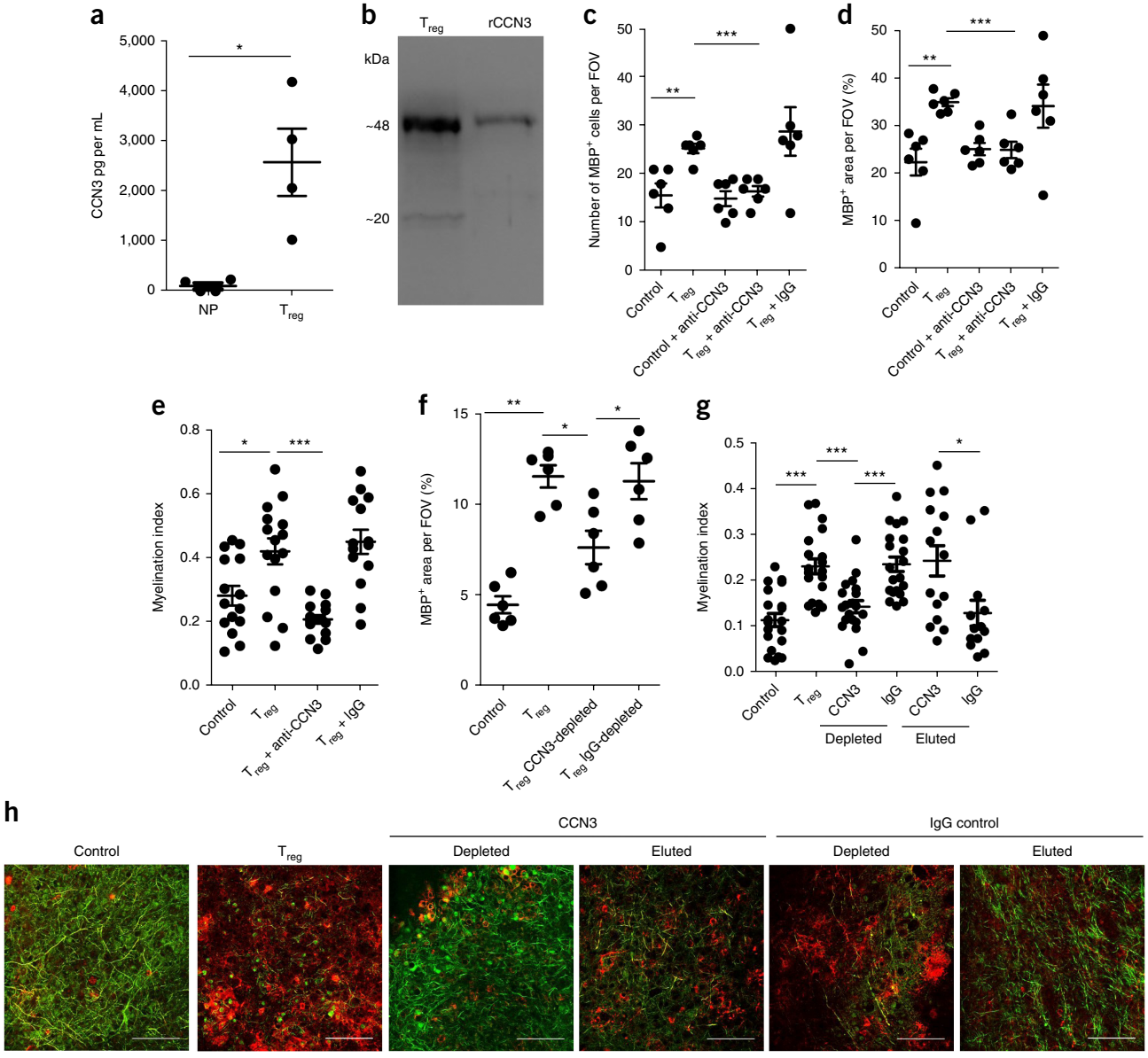

Figure 4 CCN3 is produced by T_{reg} and promotes oligodendrocyte differentiation and myelination. (**a**) ELISA quantification of CCN3 in T cell-conditioned media; $n = 4$ independently generated supernatants using different mice ($U = 0$, $P = 0.0294$, two-tailed Mann-Whitney U-test). (**b**) Western blot analysis of CCN3 in T_{reg}-conditioned medium. Recombinant CCN3 (rCCN3, 25 ng, R&D Systems) was used as a positive control. (**c**,**d**) Immunofluorescence analysis of (**c**) MBP$^+$ cell numbers (control vs. T_{reg}: $t = 3.648$, d.f. = 10, $P = 0.0045$; T_{reg} vs. T_{reg} + aCCN3: $t = 6.104$, d.f. = 10, $P = 0.0001$; unpaired two-tailed Student's t-test; T_{reg} vs. T_{reg} + IgG: $U = 10$, $P = 0.2207$; Mann-Whitney U-test) and (**d**) MBP$^+$ percentage area in mixed glial cultures, $n = 6$ wells (control vs T_{reg}: $U = 0$, $P = 0.0022$; T_{reg} vs. T_{reg} + aCCN3: $U = 0$, $P = 0.0022$; T_{reg} vs. T_{reg} + IgG: $U = 18$, $P = 1$; two-tailed Mann-Whitney U-test). (**e**) Myelination index (MBP$^+$NF200$^+$) of brain stem slices at 7 d.i.v. ($n = 15$ FOV for control, T_{reg} and T_{reg} + anti-CCN3 conditions; $n = 14$ FOV for T_{reg} + IgG condition). FOVs were from 3–6 slices per group (control vs. T_{reg}: $t = 2.739$, d.f. = 28, $P = 0.0106$; T_{reg} vs. T_{reg} + anti-CCN3: $t = 4.998$, d.f. = 28, $P < 0.0001$; unpaired two-tailed Student's t-test). (**f**) Immunofluorescence analysis of MBP$^+$ percentage area in mixed glial cultures ($n = 6$ wells; control vs. T_{reg}: $U = 0$, $P = 0.0022$; T_{reg} vs. T_{reg} CCN3-depleted: $U = 3$, $P = 0.0152$; T_{reg} CCN3-depleted vs. T_{reg} IgG-depleted: $U = 5$, $P = 0.0411$; two-tailed Mann-Whitney U-test). (**g**,**h**) Immunofluorescence analysis of (**g**) myelination index (MBP$^+$NF200$^+$) and (**h**) representative images of brain stem slices at 7 d.i.v. ($n = 20$ FOV each for control, T_{reg}, CCN3-depleted and IgG-depleted conditions; $n = 15$ FOV for CCN3-eluted condition; $n = 13$ FOV for IgG-eluted condition). FOVs were from 3 or 4 slices per group (control vs. T_{reg}: $t = 5.378$, d.f. = 38, $P < 0.0001$; T_{reg} vs. CCN3-depleted: $t = 4.159$, d.f. = 38, $P = 0.0002$; CCN3-depleted vs. IgG-depleted: $t = 4.446$, d.f. = 38, $P < 0.0001$; unpaired two-tailed Student's t-test; CCN3-eluted vs. IgG-eluted: $U = 43$, $P = 0.0129$; two-tailed Mann-Whitney U-test). Scale bar, 100 µm; green, NF200; red, MBP. Data shown are representative of at least 4 (**a**), 2 (**b** and **f**–**h**) and 3 (**c**–**e**) independent experiments. Data are presented with mean values as indicated; error bars show s.e.m.; $*P < 0.05$, $**P < 0.01$, $***P < 0.001$.

glial cells using mixed glial cultures containing OPC as well as astrocytes and microglia (**Supplementary Fig. 3a**). Treatment with T_{reg}-conditioned media for 5 d significantly increased oligodendrocyte differentiation compared to control medium (**Fig. 3a**,**b**,**d**) and control nonpolarized T cell-conditioned medium (**Supplementary Fig. 3b**,**c**), demonstrating direct T_{reg} signaling to glia. This effect was consistent independent of whether T_{reg} were induced from total $CD4^+$ T cells or from naive $CD4^+$ T cells (**Supplementary Fig. 3d**). Supporting our *in vivo* findings, we observed no difference in oligodendrocyte lineage cell numbers (**Fig. 3c**), proliferation (**Fig. 3e**,**f**) or survival (**Supplementary Fig. 3e**,**f**).

As proof of principle that T_{reg} can directly modulate a regenerative cell population, independent of other CNS cells, pure OPC were cultured in the presence or absence of T cell-conditioned media. Within just 2 d, OPC treated with T_{reg}-conditioned media exhibited significantly more MBP^+ differentiated oligodendrocytes (**Fig. 3g**,**h**), demonstrating a direct action of T_{reg} on OPC. To test whether this was functionally relevant, T_{reg}-conditioned media were added to OPC–dorsal root ganglion (DRG) neuron co-cultures. T_{reg} accelerated myelination of DRG neurons, which was evident within 4 d of stimulation with T_{reg}-conditioned media (**Fig. 3i**,**j**). Although these findings do not rule out additional indirect mechanisms, these data show that T_{reg}-secreted factors can directly signal to OPC to promote oligodendrocyte differentiation and functional myelination. This demonstrates for the first time, to our knowledge, that T_{reg} can alter the regenerative capacity of CNS progenitor cells.

CCN3 is produced by T_{reg} and promotes oligodendrocyte differentiation and myelination

We next investigated T_{reg}-secreted factors that enhanced oligodendrocyte differentiation and myelination. Analysis of conditioned media by proteome profiling identified a number of candidate factors relevant to regeneration (**Supplementary Fig. 4a**), including CCN3, a growth regulatory protein with bioactivity in extracellular, cytoplasmic and nuclear compartments and which is implicated in regeneration of various tissues[22–25]. Dual enzyme-linked immunosorbent assay (ELISA) and western blot validation confirmed that CCN3 was produced by T_{reg} (**Fig. 4a**,**b**). To determine whether CCN3 mediated the oligodendrocyte-differentiating effect of T_{reg}, anti-CCN3 antibody was added to glial and brain slice cultures treated with T_{reg}-conditioned media for 5 and 7 d, respectively. Anti-CCN3 antibody abolished T_{reg}-induced oligodendrocyte differentiation in glial cultures (**Fig. 4c**,**d** and **Supplementary Fig. 4b**) and inhibited the promyelinating effect of T_{reg} in brain slice cultures (**Fig. 4e**). To confirm these findings with a second loss-of-function approach, CCN3 was depleted from T_{reg}-conditioned media (**Supplementary Fig. 4c**,**d**) and recovered as eluted protein. T_{reg}-conditioned media depleted of CCN3 failed to promote oligodendrocyte differentiation in glial cultures (**Fig. 4f**) or brain slice myelination (**Fig. 4g**,**h**). Furthermore, treatment with recovered CCN3 significantly enhanced brain slice myelination (**Fig. 4g**,**h**). These studies implicate CCN3 as a T_{reg}-derived protein that mediates T_{reg}-driven OPC differentiation and CNS myelination.

DISCUSSION

Immune-mediated tissue regeneration is an expanding field, and recent studies highlight the importance of innate immune signaling in myelin regeneration[3,4,26]. Yet despite decades of research into T cell-mediated pathogenesis and immunomodulation of CNS demyelination, very little is known about T cell functions in remyelination. Given that T cell-targeting therapies are used in MS, it is crucial to understand the full range of roles played by T cells. However, when interrogating regenerative immune functions, appropriate choice of experimental models is crucial. T_{reg} limit damage in many inflammatory disease models, including EAE. Overlapping tissue damage and regeneration often occur in immune-mediated disease models such as EAE. Thus, true enhancement of regeneration can be challenging to distinguish from modulation of immunopathogenicity in these models. This motivated our choice of lysolecithin-induced demyelination, in which the demyelinating insult is time-limited, clearly defined anatomically, independent of immune-driven tissue damage and follows a well-defined course of highly efficient myelin regeneration. With this approach, in combination with other models without peripheral immune influence, such as OPC and brain slice cultures, we have uncovered a key regenerative function of T_{reg}. Mechanisms underlying this function include acceleration of oligodendrocyte differentiation and (re)myelination, via CCN3, a protein which, to our knowledge, was not previously known to target OPC or indeed to be produced by T_{reg}.

CCN3 is a growth-regulatory protein with bioactivity in extracellular, cytoplasmic and nuclear compartments, and it is implicated in regeneration of various tissues[23–25,27,28]. CCN3 is expressed in the developing CNS[22,29] and in glioma[30], but has not previously been implicated in CNS regeneration. Of note, we detected CCN3 expression in early organotypic brain slice cultures (data not shown); this may be developmentally regulated or due to tissue injury. In immune development, $CD34^+$ bone marrow progenitor cells express CCN3; however, to our knowledge, ours is the first report showing that T_{reg}, or indeed any T cell population, produce CCN3. Together, these findings identify CCN3 as an immune-effector molecule from early innate immune development to resolution of adaptive immune responses. This potentially places CCN3 at the leading edge of immune-mediated tissue regeneration and warrants investigation in immune cells at other anatomical sites. Notably, commercially sourced recombinant CCN3 did not induce oligodendrocyte differentiation (data not shown). This may be due to the lack of critical post-translational modifications in recombinant CCN3 and/or the presence of a 10-His tag at the C-terminus of the recombinant protein. This tag may impair bioactivity of this key functional region of CCN3, which contains a cysteine knot motif involved in homo- and heterodimerization. This emphasizes the importance of both gain-of-function and loss-of-function studies of CCN3 in reductionist and more complex models.

Recently, Burzyn *et al.* identified roles for T_{reg} in muscle regeneration associated with local immunomodulation and amphiregulin expression[9], while Arpaia *et al.* reported T cell receptor (TCR)-independent tissue-protective functions of amphiregulin-expressing T_{reg} in influenza-infected lungs[10]. Other studies describe associations of T_{reg} with regeneration of cardiac muscle and neurons[31–33]. Here we identified that T_{reg} directly promote oligodendrocyte differentiation and myelin production, even in the absence of overt inflammation. Thus, signaling from T_{reg} can directly increase the regenerative capacity of a progenitor cell population, independent of immunomodulation known to support regeneration at other anatomical sites. This confers a primary regenerative role for T_{reg} complementary to, but distinct from, known immunomodulatory functions. In concert, these two functions confer fundamental damage-limiting and damage-resolving roles to T_{reg}. Therapies to boost tissue regeneration should consider this emerging and central role of T_{reg} in natural regeneration. This knowledge holds therapeutic potential for tissue regeneration in diseases such as MS.

Collectively, our findings and recent studies by others show that T_{reg} promote regeneration via different factors in different tissues. Our regenerative immunology study expands the classical functions of T_{reg} beyond regulation to include regeneration.

METHODS

Methods, including statements of data availability and any associated accession codes and references, are available in the online version of the paper.

Note: Any Supplementary Information and Source Data files are available in the online version of the paper.

ACKNOWLEDGMENTS

We thank A. Rudensky (Memorial Sloan Kettering Cancer Centre) for providing Foxp3-DTR mice and B. Malissen (Aix Marseille Université) for the provision of Foxp3-eGFP mice. We acknowledge extensive technical support from S. Leech, S. Peoples, N. de la Vega Gallardo, S. Mitchell, J. Brown, R. Blain and the staff of the animal facility. This work was supported by the Biotechnology and Biological Sciences Research Council (BB/J01026X/1 and BB/N003721/1, to D.C.F.), The Leverhulme Trust (ECF-2014-390, to Y.D.), QUB (QUB - Lucy McGuigan Bequest, to D.C.F.), The UK Multiple Sclerosis Society (941 and 50, to R.J.M.F. and C.Z.), MRC UK Regenerative Medicine platform (MR/KO26666/1, to A.C.W.), University of Edinburgh Wellcome Trust Multi User Equipment Grant (WT104915MA, to A.C.W.), by a core support grant from the Wellcome Trust and MRC to the Wellcome Trust - Medical Research Council Cambridge Stem Cell Institute (097922/Z/11/Z to R.J.M.F.), studentship support from Dept. for the Economy (Northern Ireland) and British Pathological Society, US National Multiple Sclerosis Society (RG5203A4, to J.R.C.), NIH/NINDS (NS095889, to J.R.C.), NIH/NIGMS IRACDA Postdoctoral Fellowship (K12GM081266, to S.R.M.) and Wellcome Trust (110138/Z/15/Z, to D.C.F.).

AUTHOR CONTRIBUTIONS

Experiments were designed, performed and analyzed by Y.D., T.O.H., M.D., R.P., S.R.M., S.F., M.N., G.E., J.M., J.F., I.V.A., J.R.C. and D.C.F. Image analysis tools were developed by P.B. and P.H. EM was performed and analyzed by E.E., A.B. and A.C.W. C.Z., R.H., A.K., P.N.M., B.P., R.J.I., J.R.C. and R.J.M.F. provided advice on experimental design and interpretation, and I.V.A., P.M. and R.J.M.F. provided mentorship. Manuscript was written by Y.D. and D.C.F. with contributions from all authors. D.C.F. oversaw the study.

COMPETING FINANCIAL INTERESTS

The authors declare no competing financial interests.

1. Fünfschilling, U. *et al.* Glycolytic oligodendrocytes maintain myelin and long-term axonal integrity. *Nature* **485**, 517–521 (2012).
2. Lee, Y. *et al.* Oligodendroglia metabolically support axons and contribute to neurodegeneration. *Nature* **487**, 443–448 (2012).
3. Miron, V.E. *et al.* M2 microglia and macrophages drive oligodendrocyte differentiation during CNS remyelination. *Nat. Neurosci.* **16**, 1211–1218 (2013).
4. Ruckh, J.M. *et al.* Rejuvenation of regeneration in the aging central nervous system. *Cell Stem Cell* **10**, 96–103 (2012).
5. Bieber, A.J., Kerr, S. & Rodriguez, M. Efficient central nervous system remyelination requires T cells. *Ann. Neurol.* **53**, 680–684 (2003).
6. Woodruff, R.H., Fruttiger, M., Richardson, W.D. & Franklin, R.J.M. Platelet-derived growth factor regulates oligodendrocyte progenitor numbers in adult CNS and their response following CNS demyelination. *Mol. Cell. Neurosci.* **25**, 252–262 (2004).
7. Arnett, H.A. *et al.* bHLH transcription factor Olig1 is required to repair demyelinated lesions in the CNS. *Science* **306**, 2111–2115 (2004).
8. Ousman, S.S. & David, S. Lysophosphatidylcholine induces rapid recruitment and activation of macrophages in the adult mouse spinal cord. *Glia* **30**, 92–104 (2000).
9. Burzyn, D. *et al.* A special population of regulatory T cells potentiates muscle repair. *Cell* **155**, 1282–1295 (2013).
10. Arpaia, N. *et al.* A distinct function of regulatory T Cells in tissue protection. *Cell* **162**, 1078–1089 (2015).
11. Kim, J.M., Rasmussen, J.P. & Rudensky, A.Y. Regulatory T cells prevent catastrophic autoimmunity throughout the lifespan of mice. *Nat. Immunol.* **8**, 191–197 (2007).
12. Christiaansen, A.F., Boggiatto, P.M. & Varga, S.M. Limitations of Foxp3(+) Treg depletion following viral infection in DEREG mice. *J. Immunol. Methods* **406**, 58–65 (2014).
13. Meyer Zu Hörste, G. *et al.* Active immunization induces toxicity of diphtheria toxin in diphtheria resistant mice--implications for neuroinflammatory models. *J. Immunol. Methods* **354**, 80–84 (2010).
14. Mayer, C.T. *et al.* Advantages of Foxp3(+) regulatory T cell depletion using DEREG mice. *Immun. Inflamm. Dis.* **2**, 162–165 (2014).
15. Huang, J.K. *et al.* Retinoid X receptor gamma signaling accelerates CNS remyelination. *Nat. Neurosci.* **14**, 45–53 (2011).
16. Zhang, H., Jarjour, A.A., Boyd, A. & Williams, A. Central nervous system remyelination in culture--a tool for multiple sclerosis research. *Exp. Neurol.* **230**, 138–148 (2011).
17. Hild, W. Myelinbildung in Kulturen des Zentralnervensystems. *Verh. Anat. Ges.* **53**, 315–317 (1956-1957).
18. Birgbauer, E., Rao, T.S. & Webb, M. Lysolecithin induces demyelination in vitro in a cerebellar slice culture system. *J. Neurosci. Res.* **78**, 157–166 (2004).
19. Ling, C., Verbny, Y.I., Banks, M.I., Sandor, M. & Fabry, Z. *In situ* activation of antigen-specific CD8+ T cells in the presence of antigen in organotypic brain slices. *J. Immunol.* **180**, 8393–8399 (2008).
20. Kim, J. *et al. PINK1* deficiency enhances inflammatory cytokine release from acutely prepared brain slices. *Exp. Neurobiol.* **22**, 38–44 (2013).
21. Sheridan, G.K. & Dev, K.K. S1P1 receptor subtype inhibits demyelination and regulates chemokine release in cerebellar slice cultures. *Glia* **60**, 382–392 (2012).
22. Su, B.Y. *et al.* The expression of *CCN3* (nov) RNA and protein in the rat central nervous system is developmentally regulated. *Mol. Pathol.* **54**, 184–191 (2001).
23. Leask, A. & Abraham, D.J. All in the CCN family: essential matricellular signaling modulators emerge from the bunker. *J. Cell Sci.* **119**, 4803–4810 (2006).
24. Lin, C.G. *et al.* CCN3 (NOV) is a novel angiogenic regulator of the CCN protein family. *J. Biol. Chem.* **278**, 24200–24208 (2003).
25. Wang, X., He, H., Wu, X., Hu, J. & Tan, Y. Promotion of dentin regeneration via CCN3 modulation on Notch and BMP signaling pathways. *Biomaterials* **35**, 2720–2729 (2014).
26. Kotter, M.R., Setzu, A., Sim, F.J., Van Rooijen, N. & Franklin, R.J.M. Macrophage depletion impairs oligodendrocyte remyelination following lysolecithin-induced demyelination. *Glia* **35**, 204–212 (2001).
27. Perbal, B. NOV (nephroblastoma overexpressed) and the CCN family of genes: structural and functional issues. *Mol. Pathol.* **54**, 57–79 (2001).
28. Perbal, B. CCN proteins: a centralized communication network. *J. Cell Commun. Signal.* **7**, 169–177 (2013).
29. Le Dréau, G. *et al.* NOV/CCN3 promotes maturation of cerebellar granule neuron precursors. *Mol. Cell. Neurosci.* **43**, 60–71 (2010).
30. Xin, L.W., Martinerie, C., Zumkeller, W., Westphal, M. & Perbal, B. Differential expression of novH and CTGF in human glioma cell lines. *Clin. Mol. Pathol.* **49**, M91–M97 (1996).
31. Raposo, C. *et al.* CNS repair requires both effector and regulatory T cells with distinct temporal and spatial profiles. *J. Neurosci.* **34**, 10141–10155 (2014).
32. Saxena, A. *et al.* Regulatory T cells are recruited in the infarcted mouse myocardium and may modulate fibroblast phenotype and function. *Am. J. Physiol. Heart Circ. Physiol.* **307**, H1233–H1242 (2014).
33. Weirather, J. *et al.* Foxp3+ CD4+ T cells improve healing after myocardial infarction by modulating monocyte/macrophage differentiation. *Circ. Res.* **115**, 55–67 (2014).

ONLINE METHODS

Animals. All mice were on a C57BL/6 background and were bred in-house. Foxp3-DTR mice were a kind gift from Prof. Alexander Rudensky (Memorial Sloan Kettering Institute, New York) and Foxp3-eGFP mice were a kind gift from Prof. B. Malissen[34]. Experiments used both male and female neonatal P0–P9 pups and animals from 6–24 weeks from sources above. To deplete Foxp3$^+$ cells in Foxp3-DTR mice, diphtheria toxin was administered as described below. All animal maintenance and experiments were in compliance with the UK Home Office and approved by the University's Ethical Committee.

T_{reg} depletion and induction of lysolecithin-mediated demyelination. Male and female mice from 8 to 24 weeks of age were used. To deplete Foxp3$^+$ cells in Foxp3-DTR mice, 1 µg DT (Sigma) in 200 µl saline was injected i.p. daily for 3–4 d before demyelination. For maintenance of T_{reg} depletion, 1 µg DT was injected i.p. every third day after the demyelination procedure. Control mice were treated with saline. Depletion was routinely confirmed in blood and spleen by flow cytometry. L-α-lysophosphatidylcholine (lysolecithin; Sigma) was used to induce a focal demyelinated lesion in the spinal cord of mice as described previously[6,35]. In brief, 1.2 µL lysolecithin was injected into the ventral white matter of the lower thoracic spinal cord between vertebrae T11–12 or T12–13. At indicated timepoints, mice were terminally anesthetized with ketamine/Rompun, transcardially perfused with 4% paraformaldehyde in PBS or PBS alone (for flow cytometry studies), and the spinal cord tissue was dissected.

Adoptive transfer of wild-type T_{reg} into T_{reg}-depleted FoxP3-DTR mice. FoxP3-DTR mice were treated with DT as described above. In the 24 h before lysolecithin-induced demyelination, mice were injected i.p. with 1×10^6 MACS-purified T_{reg} from wild-type mice that were insensitive to DT treatment, using a CD4$^+$ T cell isolation kit (Stemcell Technologies).

Tissue processing. For immunohistochemistry, spinal cord tissue was postfixed for 2–4 h in 4% PFA and immersed in 20% sucrose in PBS solution overnight. For cryopreservation, spinal cords were embedded with OCT medium (VWR) and nonconsecutive 12-µm thick cryosections from the approximate center of lesions were mounted on glass slides[4].

Immunofluorescence staining of CNS tissue. After blocking with 10% goat serum (Vector Laboratories), spinal cord sections were incubated with antibodies for APC (1:100; clone CC1, Abcam), Ki67 (1:200; clone SoIA15, eBioscience) and Olig2 (1:200; cat. no. AB9610, Millipore) overnight. Secondary antibodies goat anti-rabbit AF488 (1:200; cat. no. A-11008, Life Technologies) and goat anti-rat AF594 (1:200; cat. no. A-11007, Life Technologies) were incubated for 1 h at RT (18–23 °C). For CC1 detection, acidic antigen retrieval was performed and a mouse-on-mouse immunodetection kit was used (Vector Laboratories). Nuclei were counterstained with DAPI before coverslipping with ProLong Gold Antifade (Life Technologies). Spinal cord images were acquired on a Leica DM5500 epi-fluorescence microscope.

Luxol fast blue staining of spinal cord tissue. Tissue was placed in 1:1 alcohol: chloroform solution for 10 h before dehydration in alcohol and incubation in 0.1% Luxol fast blue solution (Sigma) at 56 °C for 16 h. Tissue was rinsed and differentiated in 0.05% lithium carbonate solution for 30 s, followed by 70% alcohol for 30 s. After washing with distilled water, tissue was differentiated in 95% alcohol and twice in 100% alcohol (each 5 min) before immersing twice in xylene for 5 min and coverslipping.

Electron microscopy of spinal cord lesions. Animals were perfused with 3% glutaraldehyde, 2% paraformaldehyde, 0.1 M phosphate buffer (pH 7.4) and 0.7% (w/v) NaCl, and spinal cords were dissected and postfixed overnight. Specimen were postfixed in 1% osmium tetroxide (Agar Scientific, Stansted, UK), dehydrated, stained *en bloc* with uranyl acetate (Agar Scientific, Stansted, UK) and embedded in Durcupan resin (Sigma-Aldrich, UK). Ultrathin sections (70 nm) were cut on a Leica UCT ultramicrotome with a Diamond knife (Diatome), mounted on formvar-coated copper grids (Electron Microscopy Science) and counterstained with uranyl acetate and lead citrate. Random electron micrographs (109 micrographs from 3 mice per group) were taken from the lesions with an FEI Spirit transmission microscope with a Gatan Orius SC200B Camera. A total of 3,399 control axons and 2,076 axons from T_{reg}-depleted lesions were analyzed blindly.

Flow cytometric immunophenotyping. Fresh spinal cord tissue was dissected following transcardial perfusion with PBS, weighed and placed in Neuro Medium (Miltenyi Biotec). Medium was removed, tissues were individually passed through 70-µm strainers and washed with 30% Percoll to pellet cells, and the myelin-containing supernatant was carefully removed. Cells were resuspended in 200 µL flow cytometry staining buffer (FCSB; 1% FCS, 0.01% NaN_3 in PBS) before cell surface staining with antibodies to CD45 (clone 104; 1:400), CD11b (clone M1/70; 1:400), CD3 (clone 145-2C11; 1:200) and CD4 (clone GK1.5; 1:200), all from eBioscience. Foxp3 expression was determined in fresh cells from Foxp3-eGFP or Foxp3-GFP-DTR mice. To calculate cell numbers, singlets were identified by FSC-H versus FSC-A, and CD45$^+$ cells were gated for subsequent analyses of CD11b, CD3, CD4 and Foxp3-eGFP. Data were acquired on a FACSCanto II and analyzed using FlowJo software.

Cuprizone-induced demyelination. Eleven-week-old male C57BL/6 and FoxP3-DTR mice were fed 0.2% cuprizone (bis(cyclohexanone) oxaldihydrazone). Food (Teklad Custom Diet TD.140804, Envigo) and water were available *ad libitum*. Cuprizone feeding was maintained for 25 d to induce demyelination. Diet was then changed to normal rodent chow for additional 2 weeks to allow remyelination to occur. To deplete T_{reg}, mice were injected with DT (0.04g DT/kg) or vehicle on day 24 and day 25. T_{reg} depletion was maintained by DT administration every 3 d. Mice were killed for analysis on day 39 and were perfused transcardially with PBS followed by cold 4% paraformaldehyde. Brains were removed, postfixed overnight in 4% paraformaldehyde and cryoprotected in 30% sucrose. Coronal frozen sections of 20 µm thickness were cut using a Leica cryostat. Sections between 1 mm and −1 mm relative to bregma were collected and stained for CC1 and Olig2 as described above. The number of mature oligodendrocytes in the corpus callosum was quantified on images of 1 or 2 sections per animal with 5 animals per group. Images of the midline segment of the corpus callosum from frontal and middle sections were used to delineate the area for analysis of Olig2$^+$CC1$^+$ cells.

Black Gold II staining. Tissue sections were stained with Black Gold II (AG105, Millipore Corp, Billerica, MA) according to the manufacturer's instructions. Briefly, sections were washed in water, immersed in prewarmed Black Gold II solution and incubated at 60 °C for 15 min, followed by transfer into prewarmed 1% sodium thiosulfate at 60 °C for 5 min. Slides were rinsed three times, dehydrated, immersed in xylene for 2 min and coverslipped with mounting media.

Gene expression analyses. For qPCR, total RNA was extracted from cerebella of perfused mice with an RNeasy FFPE kit (Qiagen) using a modified protocol. Tissue was homogenized in supplied PKD buffer before treatment with proteinase K. All subsequent steps were followed according to the manufacturer's instructions. RNA purity and concentration was assessed by Nanodrop spectrophotometry. Samples were treated with DNase I (Invitrogen) before reverse transcription with Superscript IV (Invitrogen). cDNA samples were assayed in triplicate by qPCR using Fast SYBR Green (ThermoFisher Scientific) on a Roche LightCycler 480 system. Relative gene expression of *Plp1* was determined with the Pfaffl method using *Gapdh* as the internal control[36]. Primer sequences were as previously described[37]. An unpaired two-tailed Student's *t*-test was performed to assess statistical differences on ΔCt values of each condition, with a significance threshold of 0.05.

In situ hybridization of proteolipid protein (*Ppl1*) mRNA on paraformaldehyde-fixed CNS tissue was performed as previously described[38]. The plasmid containing a fragment of 801-bp *Plp* cDNA was provided by Prof I. Griffith (University of Glasgow). Briefly, sections were incubated with digoxigenin-labeled complementary RNA probes at 65 °C overnight and subjected to a standard wash protocol (50% formamide, 1× standard saline citrate, 0.1% Tween-20, 65 °C, 3 × 30 min) to remove nonspecific probe binding. The target bound probes were detected by alkaline phosphatase-conjugated anti-digoxigenin antibody (Roche Applied Science, cat. no. 11093274790) and visualized as purple precipitate after incubation in NBT/BCIP solution according to the manufacturer's instructions (Roche, Lewes, UK). The slides were dehydrated with ascending concentration of ethanol, cleared with xylene and mounted in dibutyl phthalate in xylene. Images were acquired with the Zeiss Axio Observer microscope.

T cell culture. $CD4^+$ T cells were immunomagnetically purified by negative selection (Stem Cell Technologies) from splenocytes of male and female C57BL/6 mice 6–14 weeks old and cultured in RPMI 1640 (Life Technologies) supplemented with 10% FCS, 1% penicillin/streptomycin, 1% L-glutamine, 1% HEPES, 1% sodium pyruvate, 1% nonessential amino acids and 50 nM β-mercaptoethanol (all Life Technologies). In **Supplementary Figure 3d**, naive $CD4^+$ T cells were purified using EasySep Mouse Naive $CD4^+$ T cell Isolation Kits (Stem Cell Technologies). T cells were activated with plate-bound anti-CD3 (1 μg/mL, clone 145-2C11) and soluble anti-CD28 (1 μg/ml, clone 37.51), both from eBioscience, for 3 d in nonpolarizing (no exogenous cytokine) or T_{reg}-polarizing conditions consisting of rhTGF-β (2 ng/mL, R&D Systems), rhIL-2 (10 ng/mL, eBioscience) and anti-IFN-γ (10 μg/mL, clone XMG1.2, Bioxcell). T cells were then reactivated in brain slice medium (described below) for a further 72 h, and conditioned media were harvested. Polarization of all cultures was verified by flow cytometry, and T_{reg} cultures used for experiments generally consisted of 80–90% $Foxp3^+$ T cells (see **Supplementary Fig. 2f**). For CCN3 immunoblotting, depletion and elution, cells were reactivated in serum-free X-VIVO 15 medium (Lonza).

For adoptive transfer experiments, nT_{reg} were immunomagnetically purified (Stem Cell Technologies) by negative selection of $CD4^+$ T cells followed by positive selection of $CD25^+$ cells from splenocytes and lymph nodes of C57BL/6 mice. For i.p. injection, cells were resuspended at 5×10^6 cells/mL in saline.

Organotypic brain-slice culture. Brainstem slices (300 μm) from male and female P0–2 C57BL/6 mice were prepared using a McIlwain Tissue Chopper and cultured in transwell inserts with brain-slice medium consisting of 46.6% minimum essential medium, 25% Earle's balanced salt solution, 25% heat inactivated horse serum, 1% penicillin/streptomycin, 1% glutamax (Life Technologies) and 1.4% D-glucose (Sigma). Slices were treated with 5% T cell-conditioned media and/or anti-CCN3 (10 μg/mL; clone 231216, R&D Systems), isotype control (clone 54447, R&D Systems) and/or eluate from immunoprecipitation every other day for the period defined. For remyelination studies, brainstem slices were demyelinated after 14 d in culture with lysolecithin (0.5 mg/ml, Sigma) for 16 h. Slices were washed and allowed to remyelinate for up to 14 d. For co-culture studies, 1.7×10^4 FACS-purified natural T_{reg} from Foxp3-eGFP mice were added directly on to brain stem slices in a volume of 10 μL (**Supplementary Fig. 2a**).

Staining of organotypic brain slices. Slices were fluorescently stained for myelin basic protein (MBP; 1:600, clone 12, Millipore) and axonal neurofilament-200 (NF200; 1:200, clone RT97, Millipore). After fixation in 4% paraformaldehyde for 45 min at RT, slices were blocked and permeabilized at RT for 1 h in 3% heat-inactivated horse serum (Life Technologies), 2% bovine serum albumin (Sigma) and 0.5% Triton X-100 (Sigma). Both primary and secondary antibodies (goat anti-rat AF594, cat. no. A11007; goat anti-mouse AF488, cat. no. A11001; and goat anti-mouse AF405 cat. no. A31553, 1:500; all from Life Technologies) were incubated overnight at 4 °C. Slices were mounted with ProLong Gold Antifade (Life Technologies) and imaged with a Leica TCS SP5 confocal microscope at 0.5-μm intervals over 10 μm, taking up to five fields of view (FOV) per slice, dependent on slice size. Representative images were displayed with a green lookup table (LUT) for NF200 and red LUT for MBP, applied using Leica AF software.

Electron microscopy of organotypic brain slices. Slices were immersion fixed in 4% PFA/2% glutaraldehyde in 0.1 M phosphate buffer for 24 h, washed in phosphate buffer and postfixed in 1% osmium tetroxide in 0.1 M phosphate buffer for 45 min. Samples were dehydrated in increasing concentrations of acetone and embedded in Araldite resin. Ultrathin 60 nm sections were stained in uranyl acetate and lead citrate and then viewed in a JEM1400 Transmission electron microscope (JEOL). To count the percentage of myelinated fibers per unit area of slice (at least 600 μm^2/condition), three photographs were taken from random, non-overlapping fields from each of 3 slices per condition and analyzed. To measure g-ratios, at least 35 randomly chosen axons from each of 3 slices per condition were analyzed by tracing the axonal circumference and the whole fiber circumference (using a graphics pad and pen). G-ratios were calculated by dividing these values, and data were analyzed using one-way ANOVA with Bonferroni *post hoc* tests, with $P < 0.05$ considered significant.

Mixed glial cultures. Mixed glial cells were generated from male and female P2–7 C57BL/6 pups according to the manufacturers' protocol for the Neural Tissue Dissociation Kit (P) (Miltenyi Biotec). In short, brains were dissected, cerebellum and meninges were removed, and tissue was dissociated via mechanical and papain enzyme digestion before filtration through a 40-μm strainer. Cells were plated in poly-L-lysine-coated (10 μg/ml, Sigma) 96-well flat, glass-bottomed plates (BD Falcon) at a density of 10^5 cells per well, and cultures were maintained at 37 °C, 5% CO_2. Cells were cultured for 5 d in DMEM (Life Technologies) supplemented with PDGFαα (10 ng/mL; PeproTech), 10% endotoxin-free FCS, 1% penicillin/streptomycin and 1% L-glutamine (Life Technologies). Cells were cultured for a further 2 d in neural medium (Miltenyi Biotec) supplemented with 1% penicillin/streptomycin, 1% L-glutamine, 2% B27/MACS Neuro Brew21 (Miltenyi Biotec) and PDGFαα (10 ng/ml; PeproTech). At day 7 in culture, PDGFαα was withdrawn to allow oligodendrocyte differentiation, and cells were stimulated with 5% T_{reg}-conditioned media, rCCN3, anti-CCN3 (clone 231216) or isotype control (clone 54447), all from R&D Systems, or controls for up to 5 d.

Immunofluorescence staining of mixed glial cultures. Cell cultures were fixed in 4% paraformaldehyde (pH 7.4) for 15–20 min at RT and blocked in 10% normal goat serum with 0.1% Triton X-100 for 1 h. Cells were then incubated with primary antibody overnight at 4 °C and with secondary antibodies for 1 h at RT. Cells were counterstained with DAPI for 5 min at RT. Primary antibodies used were rabbit anti-mouse Olig2 (1:200; cat. no. AB9610, Millipore), rat anti-mouse MBP (1:200; clone 12, Millipore), rat anti-mouse Ki67 (1:200; clone SoIA15, eBioscience), rabbit anti-mouse GFAP (1:200; cat. no. Z0334, Dako) and rat anti-mouse CD11b (1:200; clone M1/70, eBioscience); and secondary antibodies used were goat anti-rabbit AF488 (1:1,000; cat. no. A-11008) and goat anti-rat AF594 (1:1,000; cat. no. A-11007), both from Life Technologies. For live/dead staining, unfixed cells were stained using the LIVE/DEAD® Viability/Cytotoxicity Kit for mammalian cells (Life Technologies). Immunofluorescence was detected using an EVOS microscope at 10× magnification and $n = 6$ wells per condition, with one mean value from multiple images calculated for each well.

OPC purification. Immunopanning purification of OPC was performed as previously described[39]. Briefly, OPC were purified from male and female P7–9 mouse brain cortices. Tissue culture dishes were incubated overnight with goat IgG and IgM secondary antibodies to mouse (cat. no. 115-005-004, Jackson Laboratories) in 50 mM Tris-HCl at a final concentration of 10 μg/mL, pH 9.5. Dishes were rinsed and incubated at room temperature (RT) with primary antibodies for Ran-2, GalC and O4 from hybridoma supernatants[39]. Rodent brain hemispheres were diced and dissociated with papain (Worthington) at 37 °C. After trituration, cells were resuspended in a panning buffer (0.2% BSA in DPBS) and incubated at RT sequentially on three immunopanning dishes: Ran-2 and GalC were used for negative selection before positive selection with O4. OPC were released from the final panning dish using 0.05% Trypsin (Invitrogen). OPCs were typically 95% pure after immunopanning, with a viability of 94%.

OPC–DRG co-cultures. OPC–DRG co-cultures were prepared as previously described[39]. Briefly, DRG neurons from E15 Sprague-Dawley rats were dissociated, plated (150,000 cells per 25-mm cover glass) and purified on collagen-coated coverslips in the presence of 100 ng/mL NGF (AbD Serotec). Neurons were maintained for 3 weeks and washed with DMEM (Invitrogen) extensively to remove any residual NGF before seeding OPC. Co-cultures were grown in chemically defined medium composed of DMEM (Invitrogen) supplemented with B27 (Invitrogen), N2 (Invitrogen), penicillin-streptomycin (Invitrogen), N-acetyl-cysteine (Sigma-Aldrich) and forskolin (Sigma-Aldrich).

CCN3 quantification and depletion. Proteome profiling of conditioned media was performed using an Angiogenesis Antibody Array (R&D Systems) as per the manufacturer's instructions and identified CCN3 as a candidate protein of interest. Levels of CCN3 in T cell-conditioned media were quantified by ELISA (R&D Systems) according to the manufacturer's instructions.

T_{reg}-conditioned media were depleted of CCN3 using monoclonal anti-CCN3 antibody-coupled magnetic beads (clone 231216, R&D Systems and Thermo Scientific) or isotype control-coupled beads (clone 54447, R&D Systems). Coupling of antibody and beads was performed according to the manufacturers' instructions. In short, 1 mg of beads was incubated with 500 μg/mL of antibody solution, and the flow-through was analyzed by spectrophotometry. For immunoprecipitation, up to 1 mL of T_{reg}-conditioned media was added to 1 mg

doi:10.1038/nn.4528

of monoclonal antibody-coupled magnetic beads and incubated on a rotator at RT for 2 h, with additional vortexing of the samples every 15 min to ensure that the beads remained in suspension. The samples were then placed in a magnetic stand and CCN3-depleted T_{reg}-conditioned media and isotype-treated controls were collected. To elute T_{reg}-derived CCN3, beads were washed and elution buffer (0.1 M glycine, pH 2.0) was added for 3–5 min at RT. To neutralize the low pH of the solution, neutralization buffer (1 M Tris, pH 7.4) was immediately added, samples were placed on a magnetic stand and the eluate containing T_{reg}-derived CCN3 was collected and resuspended in medium according to the initial volume. Eluted product from anti-CCN3-coated and IgG-coated beads was added to brain-slice cultures as indicated.

Immunoblotting of CCN3. T cell-conditioned media or recombinant CCN3 (R&D Systems) were enriched for CCN3 using heparin-sepharose beads as previously described[40]. In short, up to 10 mL of T_{reg}-conditioned media (equivalent to 25 ng of CCN3) or recombinant CCN3 were added to 100 µL 50% heparin-sepharose slurry and incubated on a rotator at 4 °C overnight. Fifty µL of PBS-washed CCN3-bound heparin-sepharose beads were boiled and added 12.5 µL of 5× reducing loading dye for 10 min before loading on a reducing 15% SDS-PAGE. Following transfer onto PVDF membrane (Millipore) and blocking (3% BSA in PBS/1% Tween) for 1 h at RT, protein was probed using polyclonal anti-CCN3 antibody (1:1,000; cat. no. AF1976, R&D Systems) overnight at 4 °C and secondary anti-goat HRP (1:3,000; cat. no. sc-2020, Santa Cruz) for 1 h at RT.

Image analysis and data processing. Customized ImageJ[41] plugins were used to assist quantifying positively stained cells and areas in all models.

Regions of interest corresponding to spinal cord lesions were initially drawn using the polygon tool. Regions were subsequently refined based on the local cell density by thresholding a Gaussian-smoothed duplicate of the DAPI channel to give a more detailed contour, which was corrected manually if necessary using a brush selection tool. Cells were then counted manually within the lesion; in some cases, counts were automatically initialized as localized regions of high fluorescence detected by the 'find maxima' command in ImageJ before manual verification and correction to ensure that all regions contributing to the final counts were consistent with expected cell morphology (i.e., no artifacts). ImageJ plugins were written to perform the lesion refinement and to assist with manual cell counting.

Myelination index was used for overlapping myelin and axonal markers in 3D, indicating (re)myelination. Confocal *z*-stacks of brain slices, both red (MBP) and green (NF200) channels, were preprocessed by first smoothing with a 3D isotropic Gaussian filter (sigma = 0.5 µm) before subtracting a background estimate created by applying a 3D morphological opening (filter radius = 1 µm). The processed channels were then thresholded, with the threshold determined automatically by implementing the 'triangle' method in ImageJ. The overlap coefficient was determined as the proportion of above-threshold pixels in the green channel that were also detected in the red channel, which quantified MBP signals colocalizing with NF200 signals. An ImageJ plugin was written to fully automate the above steps. MBP^+ oligodendrocytes were counted manually.

Cell counts of $Olig2^+$, MBP^+ and $Ki67^+$ cells in mixed glial cultures were performed manually. MBP^+ areas were determined from the number of above-threshold pixels after applying a small median filter (radius = 1.5 pixels), followed by subtracting a background image generated by the 'subtract background' command in ImageJ (sliding paraboloid option, radius = 100 pixels). For each plate, the threshold was determined and the same threshold was applied to all analyzed images within each experiment. An ImageJ plugin was written to automate the above steps. Plugin codes will be made publically available on the Queen's University Belfast website.

Experimental designs and statistical analyses. No statistical methods were used to predetermine sample sizes, but our sample sizes were similar to those reported in previous publications[3,15,39]. For *in vivo* studies, any animal that reached a predefined welfare limit before the analysis timepoint was excluded from the study. For organotypic brain slice experiments, slice integrity was determined by neurofilament 200 (NF200) staining before analysis. Animals and brain slices were randomly assigned to experimental groups at the beginning of experiments. Myelination indices (brain slices) and MBP area (glial cultures) were blindly assessed by a computer program and in an identical manner for all files. MBP^+ cell counts in brain slices were performed by independent observers on randomly selected images from *z*-stacks. For all other studies, data collection and analyses were not performed blind to the conditions of the experiments. Datasets were tested for normal distribution, variances and statistical significance using unpaired two-tailed Student's *t*-tests for parametric data with or without Welch corrections, or using Mann-Whitney *U*-tests for nonparametric data, as detailed in figure legends. Normality of datasets was tested using the KS or D'Agostino-Pearson omnibus normality test methods. Where *n* was not sufficient for normality testing, non-normal distribution was assumed and nonparametric statistical testing was used. All statistical analysis and graphing of data were performed using GraphPad Prism. Species validation information for antibodies can be obtained from the commercial suppliers indicated.

A **Supplementary Methods Checklist** is available.

Data and code availability. The data and analysis code that support the findings of this study are available from the corresponding author upon reasonable request.

34. Wang, Y. *et al.* Th2 lymphoproliferative disorder of *LatY136F* mutant mice unfolds independently of TCR-MHC engagement and is insensitive to the action of Foxp3+ regulatory T cells. *J. Immunol.* **180**, 1565–1575 (2008).
35. Hall, S.M. The effect of injections of lysophosphatidyl choline into white matter of the adult mouse spinal cord. *J. Cell Sci.* **10**, 535–546 (1972).
36. Pfaffl, M.W. A new mathematical model for relative quantification in real-time RT-PCR. *Nucleic Acids Res.* **29**, e45 (2001).
37. Liu, J. *et al.* Impaired adult myelination in the prefrontal cortex of socially isolated mice. *Nat. Neurosci.* **15**, 1621–1623 (2012).
38. Zhao, C., Li, W.W. & Franklin, R.J. Differences in the early inflammatory responses to toxin-induced demyelination are associated with the age-related decline in CNS remyelination. *Neurobiol. Aging* **27**, 1298–1307 (2006).
39. Mei, F. *et al.* Micropillar arrays as a high-throughput screening platform for therapeutics in multiple sclerosis. *Nat. Med.* **20**, 954–960 (2014).
40. Chevalier, G. *et al.* novH: differential expression in developing kidney and Wilm's tumors. *Am. J. Pathol.* **152**, 1563–1575 (1998).
41. Schneider, C.A., Rasband, W.S. & Eliceiri, K.W. NIH Image to ImageJ: 25 years of image analysis. *Nat. Methods* **9**, 671–675 (2012).